ICFDP8-EG-176

Three-Dimensional Computational Model for Flow in an Over-expanded Nozzle with Porous Surfaces

K.S. Abdol-Hamid
NASA Langley Research Center, Hampton VA 23681

Alaa Elmiligui
Analytical Services & Materials, Inc. Hampton, VA 23666

Craig A. Hunter
NASA Langley Research Center, Hampton VA 23681

Steven J. Massey
Eagle Aeronautics, Inc., Hampton, VA 23669

ABSTRACT

A three-Dimensional computational model is used to simulate flow in a non-axi-symmetric, convergent-divergent nozzle incorporating porous cavities for shock-boundary layer interaction control. The nozzle has an expansion ratio (exit area/throat area) of 1.797 and a design nozzle pressure ratio of 8.78. Flow fields for the baseline nozzle (no porosity) and for the nozzle with porous surfaces of 10% openness are computed for Nozzle Pressure Ratio (NPR) varying from 1.29 to 9.54. The three dimensional computational results indicate that baseline (no porosity) nozzle performance is dominated by unstable, shock-induced, boundary-layer separation at over-expanded conditions. For NPR≤1.8, the separation is three dimensional, somewhat unsteady, and confined to a bubble (with partial reattachment over the nozzle flap). For NPR≥2.0, separation is steady and fully detached, and becomes more two dimensional as NPR increased. Numerical simulation of porous configurations indicates that a porous patch is capable of controlling off design separation in the nozzle by either alleviating separation or by encouraging stable separation of the exhaust flow. In the present paper, computational simulation results, wall centerline pressure, mach contours, and thrust efficiency ratio are presented, discussed and compared with experimental data. Results indicate that comparisons are in good agreement with experimental data. The three-dimensional simulation improves the comparisons for over-expanded flow conditions as compared with two-dimensional assumptions.

INTRODUCTION

A clear understanding of the flow in an over-expanded nozzle with porous surfaces is important because it sheds light on the complicated relationship between over-expansion, shock-induced separation, passive control, and thrust efficiency. An accurate tool to model the above mentioned phenomena is of critical importance. Investigations in the area of Passive Porosity Technology (1-10) for propulsion applications have led to an increased interest in upgrading the Computational Fluid Dynamics code PAB3D's (10-12) modeling capabilities. PAB3D is a structured, multi-block, parallel, implicit, finite-volume solver of three-dimensional, unsteady, Reynolds-Averaged Navier-Stokes equations. Advanced turbulence models are available in PAB3D and are widely used in internal and external flow applications by NASA and the U.S. aerospace industry. Second-order time accuracy can be achieved by employing physical time sub-iteration and dual time sub-iteration (13). Porous boundary simulates a porous surface placed above a plenum. The model eliminates the need for construction of a grid within an underlying plenum, thereby simplifying the numerical modeling of passively porous control systems (9,10).

Asbury & Hunter (2-3) performed an experimental investigation on a non axi-symmetric, convergent-divergent nozzle incorporating porous cavities for shock-boundary layer interaction control. The experimental testing on the nozzle is performed at the NASA Langley 16-Foot Transonic Tunnel Complex as part of a comprehensive static performance investigation. High pressure is used to simplify the jet. Force, moment, and pressure measurements are made and Schlieren flow visualization is obtained for a subscale, non-axi-symmetric, two-dimensional, convergent divergent nozzle. Details of the nozzle are shown in Figure 1, and a photograph of the nozzle is shown in Figure 2.

Hunter (5) conducted an experimental study and showed that over-expanded nozzle flow is dominated by shock-induced boundary-layer separation that is divided into two distinct flow regimes: three-dimensional separation with partial reattachment and a fully detached two-dimensional separation. For NPR≤1.8, the separation is three dimensional, somewhat unsteady, and confined to a bubble (with partial reattachment on the nozzle flap). For NPR≥2.0, separation is steady and fully detached from nozzle flap. As NPR increased nozzle flow exhibited less and less 3 dimensional (3D) character. When NPR increased from 1.8 to 2.0, the nozzle goes through a dramatic transition, dividing the two separated flow regimes. With the implementation of a porous boundary condition in PAB3D (6), a detailed numerical investigation of the nozzle is conducted, and numerical results are in good agreement with experimental data of ref. (3), however, the two-dimensional (2D) computational model fails to accurately simulate the flow for the lower NPR values (below 2.0). The highly 3D nature of the flow is the reason for the discrepancy with 2D calculations. This suggests that a three dimensional computation is needed to correctly model separated nozzle flow.

In the present study, a three dimensional computational model is used to study the flow of a rectangular, convergent divergent nozzle. Comparison between the 2D and 3D computational model are presented with detailed analysis on why the 2D computational model, ref. (6), fails to predict the flow field for low NPRs.

The organization of the paper is as follows: The governing equations and boundary conditions are presented followed by a detailed computational study of a convergent-divergent nozzle incorporating porous cavities. Numerical results for both the baseline configuration and porous configurations are presented, discussed and compared to experimental data.

COMPUTATIONAL FLUID DYNAMICS SIMULATION

In this study, the PAB3D code is used in conjunction with two-equation k-ε turbulence closure and nonlinear algebraic Reynolds stress models to simulate separated nozzle flows. PAB3D has been well tested and documented for the simulation of aero-propulsive and aerodynamic flows involving separation, mixing, and other complicated phenomena, ref. (10-13). PAB3D has been ported to a number of platforms and offers a combination of good performance and low memory requirements. In addition to its advanced preprocessor, which can handle complex geometries through multi-block general patching, PAB3D has a runtime module capable of calculating aerodynamic performance on the fly and a postprocessor used for follow-on data analysis (14). PAB3D solves the simplified Reynolds-averaged Navier-Stokes equations in conservative form, obtained by neglecting stream-wise derivatives of the viscous terms. Viscous models include coupled and uncoupled simplified Navier-Stokes and thin layer Navier-Stokes options.

Roe`s upwind scheme is used to evaluate the explicit part of the governing equations, and van Leer's scheme is used for the implicit part. Diffusion terms are centrally differenced, inviscid terms are upwind differenced, and two finite volume flux-splitting schemes are used to construct the convective flux terms. PAB3D is third order accurate in space and first-order accurate in time.

GOVERNING EQUATION

The governing equations solved in this study are the time-averaged Reynolds Averaged Navier-Stokes (RANS), and the perfect gas law is chosen to represent the air properties. The full equations are listed in reference (18). Three turbulence models are used in the current study to model turbulence: a standard k-ε model (12), and two algebraic stress models: Shih-Zhu-Lumley (SZL) (16), and Girimaji model (17). The two algebraic stress models give inherently better results than the linear stress model because of the explicit modeling of effects such as relaxation, and the specific inclusion of nonlinear anisotropic effects from the mean flow strain and vorticity. With a nonlinear model, the calculation of six independent, realizable Reynolds stress terms is possible. This type of detail is important for simulating complicated multidimensional flows. A compilation of the parameters used in the turbulence models can be found in reference (18).

COMPUTATIONAL DOMAIN

The two-dimensional grid used by the authors of reference (6), is extended to a three dimensional grid. The 2D grid consisted of 66,400 cells and 5 blocks. The 3D grid has 8,062,976 cells and 41 blocks, and is shown in Figure 3. Relative to the nozzle exit, the grid extended approximately 30 throat heights downstream, 25 throat heights upstream, and 25 throat heights normal to the jet axis. In an attempt to capture the complicated physics of the shock-boundary layer interaction process, the divergent section of the nozzle is densely gridded with cells having an aspect ratio near 1:1. The boundary layer grid had 40 cells with first cell height of approximately y+=0.5. An inflow duct (sized like the instrumentation duct used in the experimental study) is located upstream of the nozzle. Reference (6) demonstrates numerical verification for PAB3D with respect to grid distribution for the 2D grid that is used in the present paper as basis for the 3D grid.

INITATIAL AND BOUNDARY CONDITIONS

Stagnation conditions are applied to the inflow duct upstream of the nozzle, and are chosen to match experimental conditions for total pressure and temperature (3). In addition, an initial Mach number is specified in the inflow block and nozzle to start the solution. The static ambient region surrounding the nozzle is defined by a subsonic condition (T_a=530°R, P_a=14.85psi, Ma=0.025) on the inflow face, a characteristic boundary condition on the top face, and a smart boundary condition on the exit face that switches between

constant pressure outflow (subsonic) and first order extrapolation (supersonic), depending on the local Mach number. All solid walls are treated as no-slip adiabatic surfaces, and the bottom of the entire domain is defined by a symmetry boundary condition.

A porous boundary condition is specified for the porous surface and porous cavity. This condition simulates a porous surface placed above a plenum. This eliminates the need for construction of a grid within an underlying plenum, thus simplifying the numerical modeling of passive porous flow control systems, and reducing computation cost, ref. (6). A sketch showing the porous cavity concept for shock-boundary layer interaction control is shown in Figure 4. The porous patch allows the high-pressure region behind the shock to communicate with the low-pressure region ahead of the shock, which reduces the shock strength and consequently reduces adverse effects of shock on the boundary layer separation.

RESULTS

Computational simulations are performed at nozzle pressure ratios from 1.26 to 9.5 for the baseline configuration "no porosity" and for nozzle with a 10% open porosity ratio patch. These conditions are chosen for detailed comparison with experimental data (3). Numerical results are presented in terms of internal flow features, static pressure, thrust performance, mach contours and Schlieren flow visualization. Grid sequencing is used to accelerate convergence by solving 1/4 then 1/2 of the grid in each of the three computational directions. Each grid level is run to convergence and compared integrated forces and flow quality with experimental data.

Figure 5 shows comparison between the present 3D and previous 2D computational results (ref 6) as well as thrust coefficient from the experimental data (ref 3). For this comparison, the Girimaji turbulence model is used. For NPR >4, the 3D result does not change from the 2D results. This indicates that the friction drag from sidewalls is not significant and that three-dimensional effect is minimum. For 2<NPR<4, 3D results are in generally better agreement with experimental data. The low NPR region (NPR<2) is obviously quite difficult to predict and 3D does not improve the predictions.

Figure 6 shows a comparison between the present 3D and 2D computational model results (ref 6) as well as experimental centerline static pressures (P/Poj), plotted against non-dimensional stream-wise location for the baseline nozzle configuration at off-design nozzle conditions for NPR= 1.41 and 2.21. CFD results are shown as the solid and dashed lines, while symbols represent experimental data of ref. (5). For low NPR=1.41, the 3D simulation improves the comparison with the experimental data from previous 2D result. Based on these results, the sidewall does amplify the 3D effect of the flow for NPR <2. For NPR=2.21. The three-dimensional effect is minimum.

Figure 7 shows comparison between kε, Girimaji and SZL turbulence models as well as thrust coefficient from the experimental data (ref 3) for the baseline configuration.

Girimaji turbulence model is in better agreement with experimental data for NPR>2.1. However, all three turbulence models fail to predict the experimental data for 1.4<NPR<2.1. Figure 8 shows a comparison between the three turbulence models results and experimental centerline static pressures (P/Poj), plotted against non-dimensional stream-wise location for the baseline nozzle configuration at off-design nozzle conditions for NPR= 1.41 and 2.21. For NPR=1.41, kε and Girimaji are in better good agreement with experimental data. The SZL turbulence model overpredicts the pressure distribution at this NPR. However for NPR = 2.21 Girimaji and SZL give better agreement with the data. In general, the Girimaji turbulence model produces the best comparisons with the experimental data for the entire NPR range.

Experimental and computational Schlieren flow visualization is shown in Figure 9 Results are representative of classic convergent-divergent nozzle flow. Schlieren flow visualization at NPR=2.0 shows the nozzle shock with a pronounced lambda foot system and fully detached separation extending from the leading lambda shock downstream past the nozzle exit. Increasing NPR forced the lambda shock to increase in size and move downstream. By NPR=3.4, the lambda shock foot had grown significantly, such that the main shock and trailing lambda foot are outside the physical nozzle, as shown in Figure 9. At this NPR, flow past the separation point showed strong resemblance to externally over-expanded flow; the jet plume necked down between the leading and trailing lambda foot, and there is an expansion fan emanating from each trailing lambda foot as it intersects the free shear layer. Figure 9 shows good qualitative agreement between computational and experimental Schlieren images, though the computational simulation is seen to predict more of a "stretched" shock structure. With increasing NPR, the leading lambda foot worked its way out of the nozzle, and pressure data and flow visualization show the nozzle to be internally shock-free. The difference between turbulence model results could be explained from the Mach contours for nozzle flow as presented in Figure 10. For NPR=1.41, the kε turbulence model gives larger pressure gradient at the throat (x=1) compared with the other results. For NPR=2.21, there is not much different between the results produced by the three turbulence models.

Figure 11 shows a comparison between kε, Girimaji and SZL turbulence models results as well as thrust coefficient from the experimental data (ref 3) for the 10% porosity configuration. The Girimaji turbulence model is in better agreement with experimental data for NPR>2.1. However, all three turbulence models fail to predict the experimental data for 1.4<NPR<2.1. Figure 12 shows comparison between kε and Girimaji turbulence models results and experimental centerline static pressures (P/Poj), plotted against non-dimensional stream-wise location for the baseline nozzle configuration at off-design nozzle conditions for NPR= 1.41 and 2.21. For NPR=1.41, kε and Girimaji are not good agreement with experimental data. For NPR=1.41, neither the use of a three-dimensional model or additional turbulence models helps to

elevate the discrepancy between the computed results and the experimental data. However for NPR = 2.21, the Girimaji turbulence mode produce better agreement with the data.

A Comparison of computed wall pressure distribution for baseline configuration and a 10% porous patch configuration, for NPR=2.21, is shown in Figure 13. At this NPR, the shock location moved to the very upstream end of the porous patch, porosity provided little apparent separation control and the only significant difference in the static pressure ratio distributions between the porous configuration and the baseline configuration is a more gradual compression through the shock for the porous configuration.

SUMMARY

This paper presents results of using two- and three-dimensional simulations of non-axisymmetric, convergent-divergent nozzle. Three-dimensional computational results are in generally good agreement with experimental data for a wide range of NPRs (NPR=2.0). Algebraic turbulence models produce accurate pressure distribution as compared with the linear kε model for a wider range of NPR. Neither the use of a three-dimensional grid nor additional turbulence models improves the computational results significantly for 1.41<NPR<2.1 range.

REFERENCES

1. Craig A. Hunter, Sally A. Viken, Richard M. Wood, and Steven X. S. Bauer. "Advanced Aerodynamic Design Of Passive Porosity Control Effectors". AIAA Paper 2001-249, Jan. 2001

2. Scott C. Asbury, Christopher L. Gunther , and Craig A. Hunter. "A passive cavity concept for improving the off-design performance of fixed-geometry exhaust nozzles." AIAA Paper 1996-2541

3. Scott C. Asbury, and Craig A. Hunter. "Static performance of a fixed-Geometry Exhaust Nozzle Incorporating Porous Cavities for Shock-Boundary Layer Interaction". NASA TM-1999-209513

4. Hunter, C.A. "Experimental, Theoretical, and Computational Investigation of Separated Nozzle Flows." AIAA Paper 1998-3107, 1998

5. Hunter, C.A. ""Experimental Investigation of Separated Nozzle Flows." Journal of Propulsion and Power. Volume 20, Number 3, 527-532

6. Elmiligui, A., Abdol-Hamid, K.S., Hunter, C.A. "Numerical Investigation Flow in an Over-expanded Nozzle with Porous Surfaces" 41st AIAA/ASME/SAE/ASEE Joint Propulsion Conference &

7. Exhibit, Tucson, Arizona, Jul 10-13, 2005, Tucson, Arizona, AIAA 2005-4159

7. J. Lopera, T. Terry, M. Patel. "Experimental Investigations of Reconfigurable Porosity for Aerodynamic Control." 2nd AIAA Flow Control Conference, Portland, Oregon, June 2004. AIAA-2004-2695.

8. M. Patel, J. DiCocco, T. Prince, T. Ng. " Flow Control Using Reconfigurable Porosity ." 21st AIAA Applied Aerodynamics Conference, Orlando, Florida, June 23-26, 2003, AIAA-2003-3665.

9. Ana F. Tinetti. "On the Use of Surface Porosity to Reduce Wake-Stator Interaction Noise." Ph.D. Thesis, Virginia Polytechnic Institute and State University, September 2001.

10. Neal T. Frink; Daryl L. Bonhaus; Veer N. Vatsa; Steven X. S. Bauer; Ana F. Tinetti. "Boundary Condition for Simulation of Flow Over Porous Surfaces" Journal of Aircraft, Vol. 40, Number 4, 2003, pp. 692-698.

11. PAB3D Code Manual Originally developed by the Propulsion Aerodynamics Branch, now under cooperative program between the Configuration Aerodynamics Branch, NASA Langley Research Center and Analytical Services & Materials, Inc. Hampton, VA. See http://www.asm-usa.com/software/pab3d.html

12. Abdol-Hamid, K.S. "Implementation of Algebraic Stress Models in a General 3-D Navier-Stokes Method (PAB3D)". NASA CR-4702, December 1995.

13. Massey, S.J., & Abdol-Hamid, K.S, "Enhancement and Validation of PAB3D for Unsteady Aerodynamics," AIAA Paper 2003-1235, 2003.

14. Massey, S. J., POST Code Manual, See http://eagle.com/post/

15. Leavitt, L.D., and Re, R.J. "Static Internal Performance Including Thrust Vectoring and Reversing of Two-Dimensional Convergent-Divergent Nozzles". NASATP-2253, 1984.

16. Shih, T.H., Zhu, J., and Lumley, J.L. "A New Reynolds Stress Algebraic Equation Model". NASA TM-106644, August 1994.

17. Girimaji, S.S. "Fully-Explicit and Self-Consistent Algebraic Reynolds Stress Model". ICASE 95-82, December 1995.

18. Carlson, J. R., "Applications of Algebraic Reynolds Stress Turbulence Models," Journal of Propulsion and Power, Volume 13, Number 5, 1997.
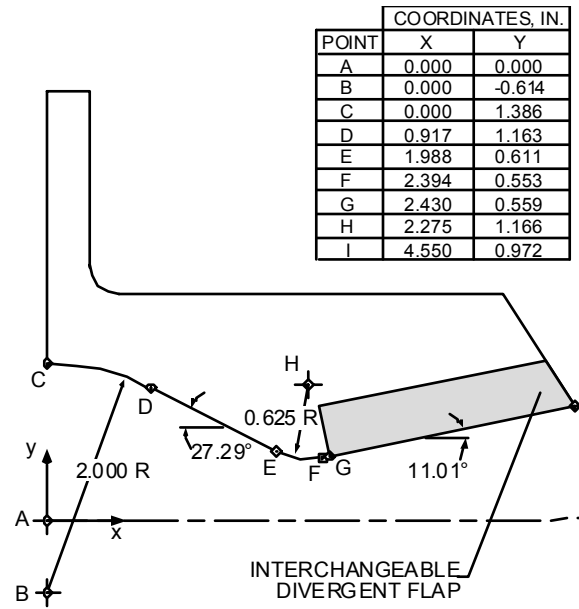
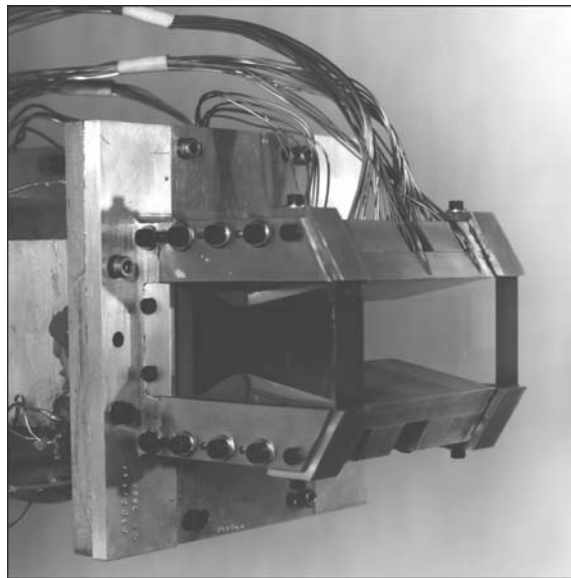| POINT | COORDINATES, IN. | |
	X	Y
A	0.000	0.000
B	0.000	-0.614
C	0.000	1.386
D	0.917	1.163
E	1.988	0.611
F	2.394	0.553
G	2.430	0.559
H	2.275	1.166
I	4.550	0.972

Figure 1 Sketch Showing Nozzle Geometric Details, ref. (3)

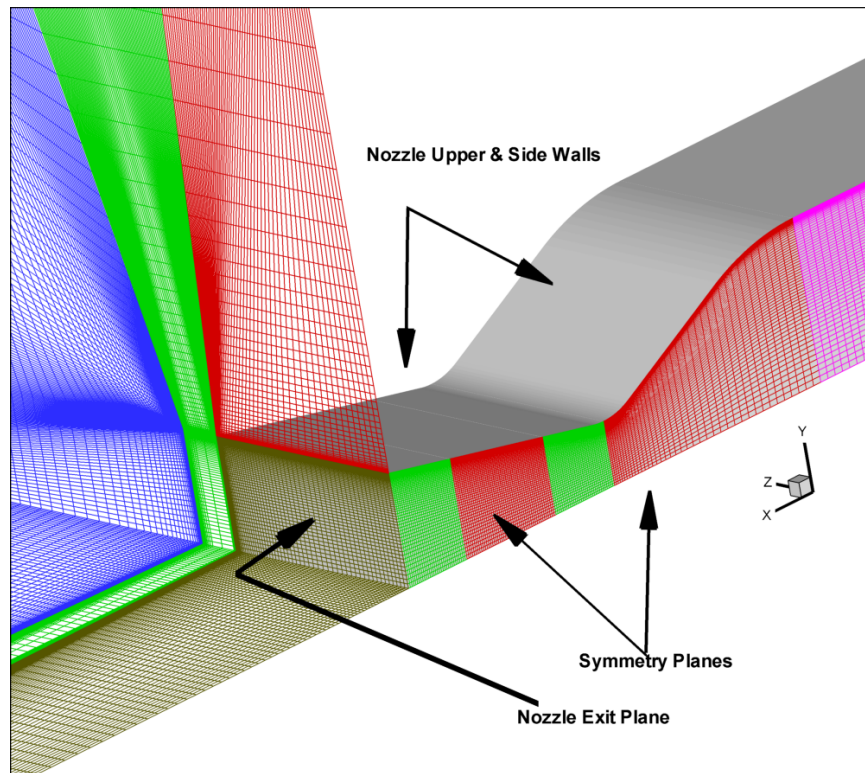**Figure 2 Non-axisymmetric Convergent-divergent Nozzle, ref. (5)**
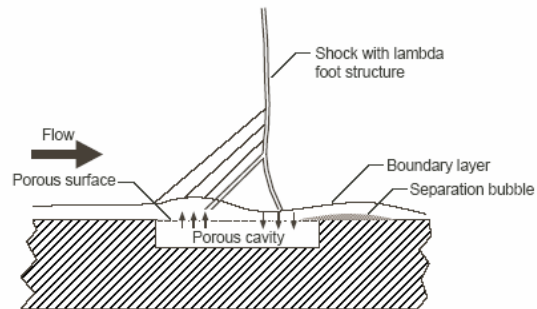
Figure 3 Three-dimensional Presentation of Computational Grid

Figure 4 Sketch showing the porous cavity concept for shock-boundary layer interaction control. ref (3)
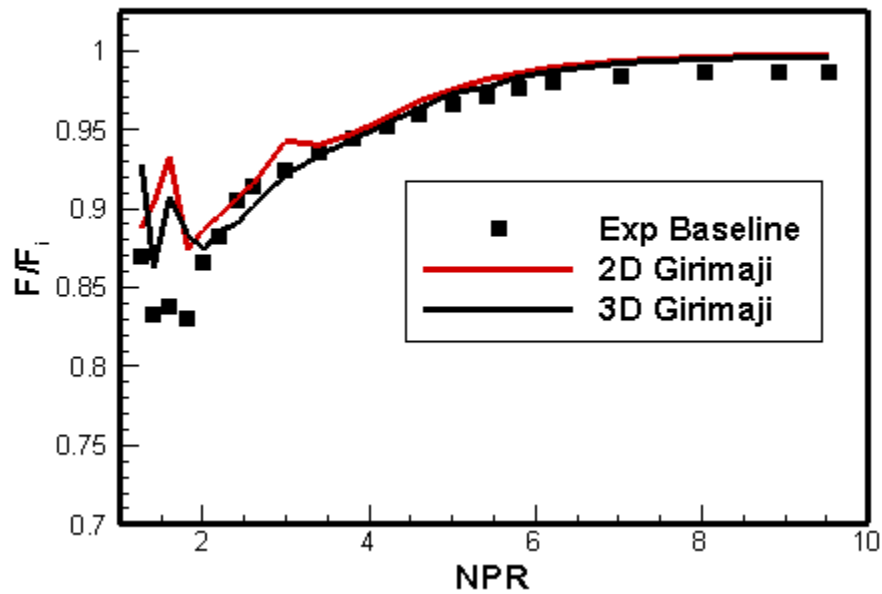
Figure 5 Comparison of Nozzle thrust coefficient for baseline configuration using 2D and 3D simulations and experimental data of ref(3)
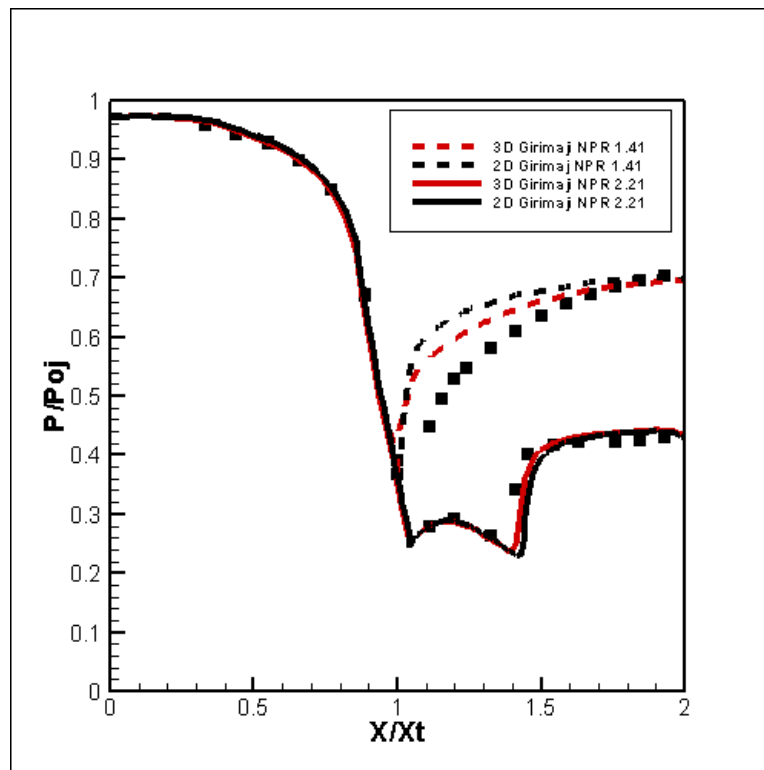
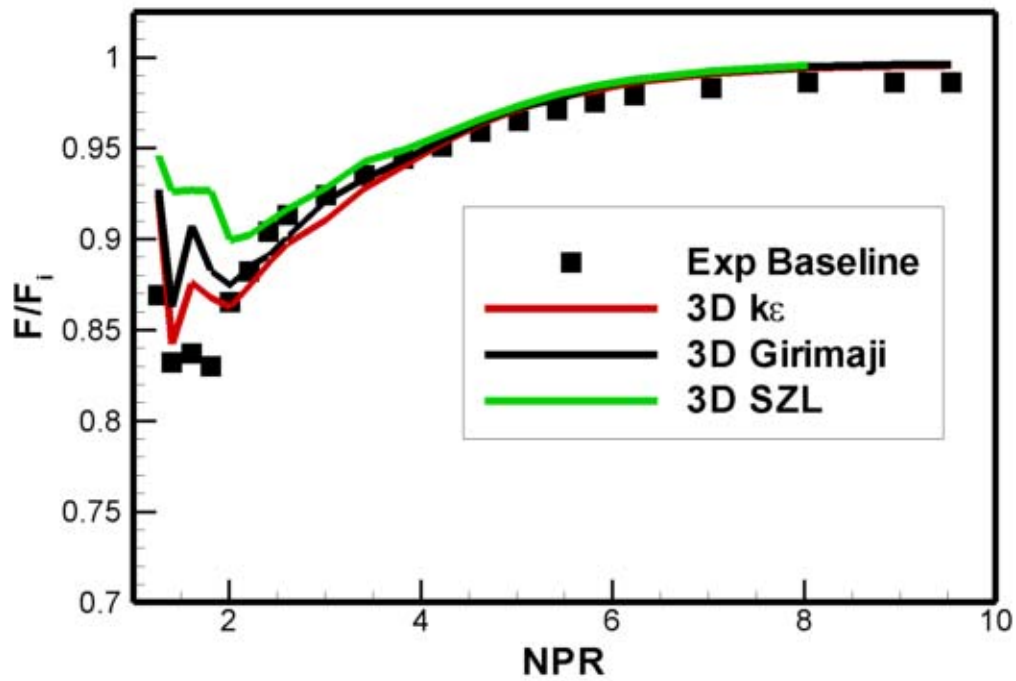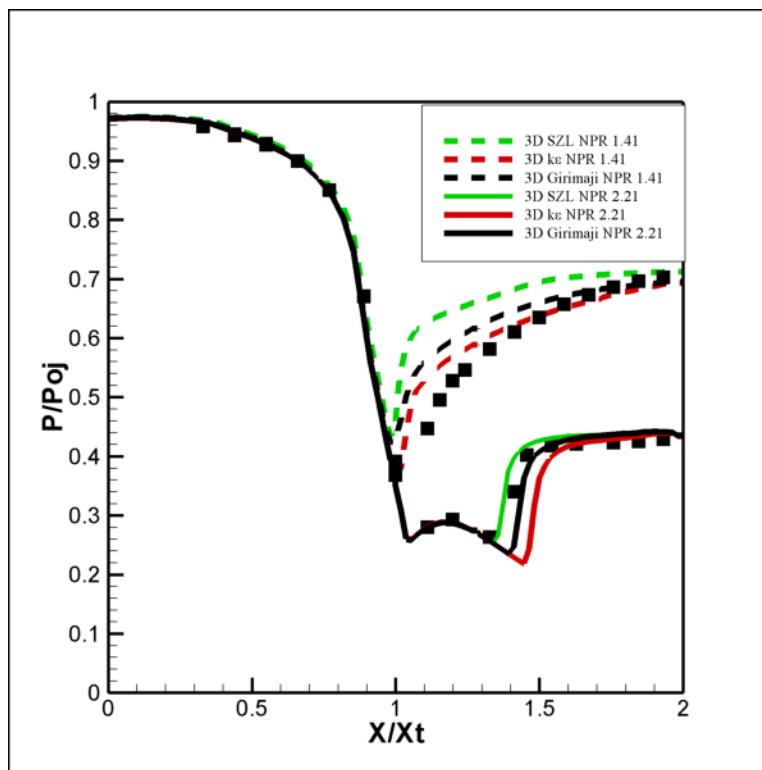**Figure 6 Comparison of 3D and 2D Computational Pressure Data and Experimental Data of ref (3) for baseline configuration.**

Figure 7 Comparison of Nozzle thrust coefficient for baseline configuration using different turbulence models and experimental data of ref (3)

Figure 8 Comparison of turbulence models Computational Pressure Data and Experimental Data of ref (3) for baseline configuration
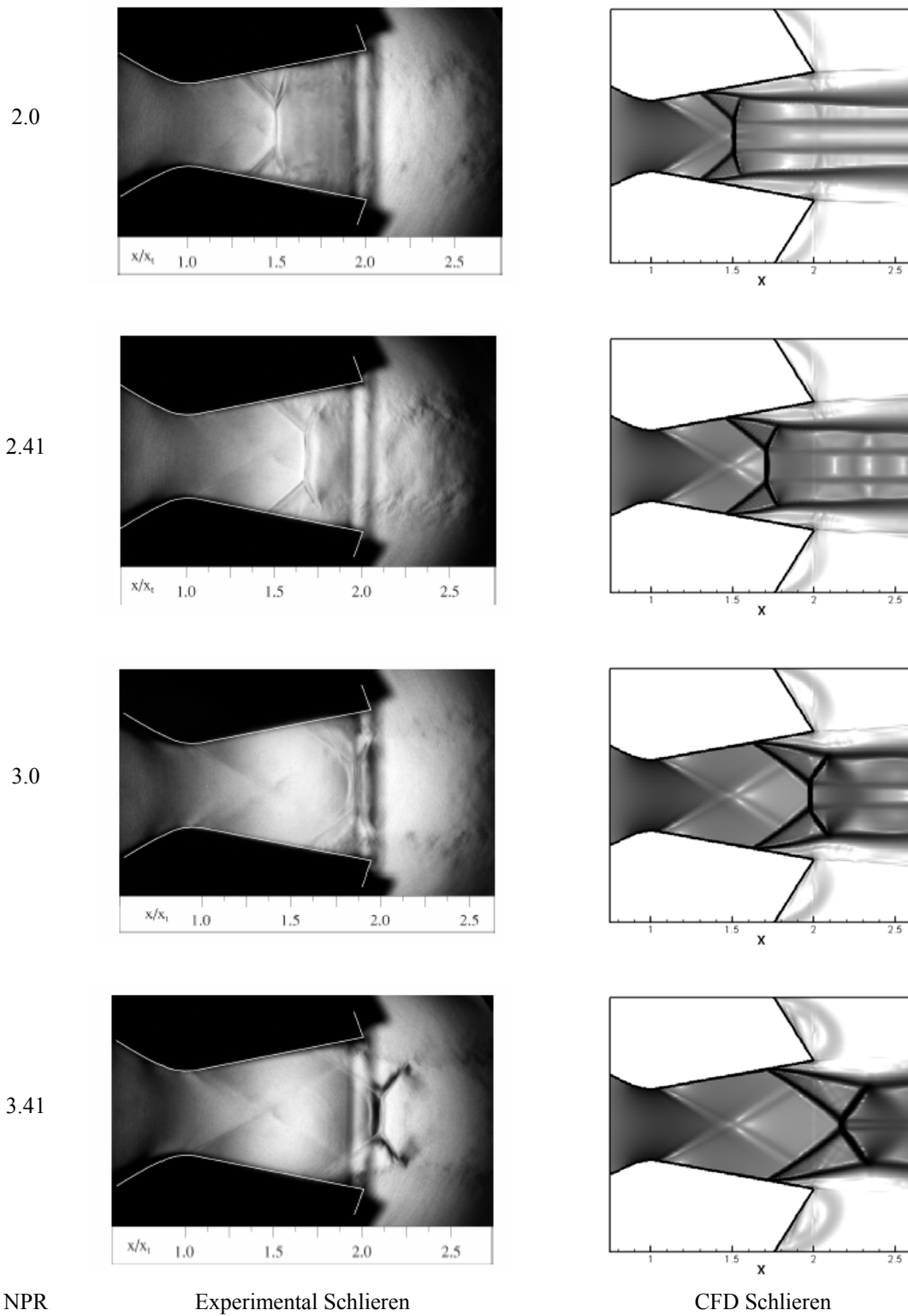
2.0		
2.41		
3.0		
3.41		
NPR	Experimental Schlieren	CFD Schlieren

Figure 9 Comparisons of experimental (ref 4) and computational Schlieren images for baseline nozzle configuration

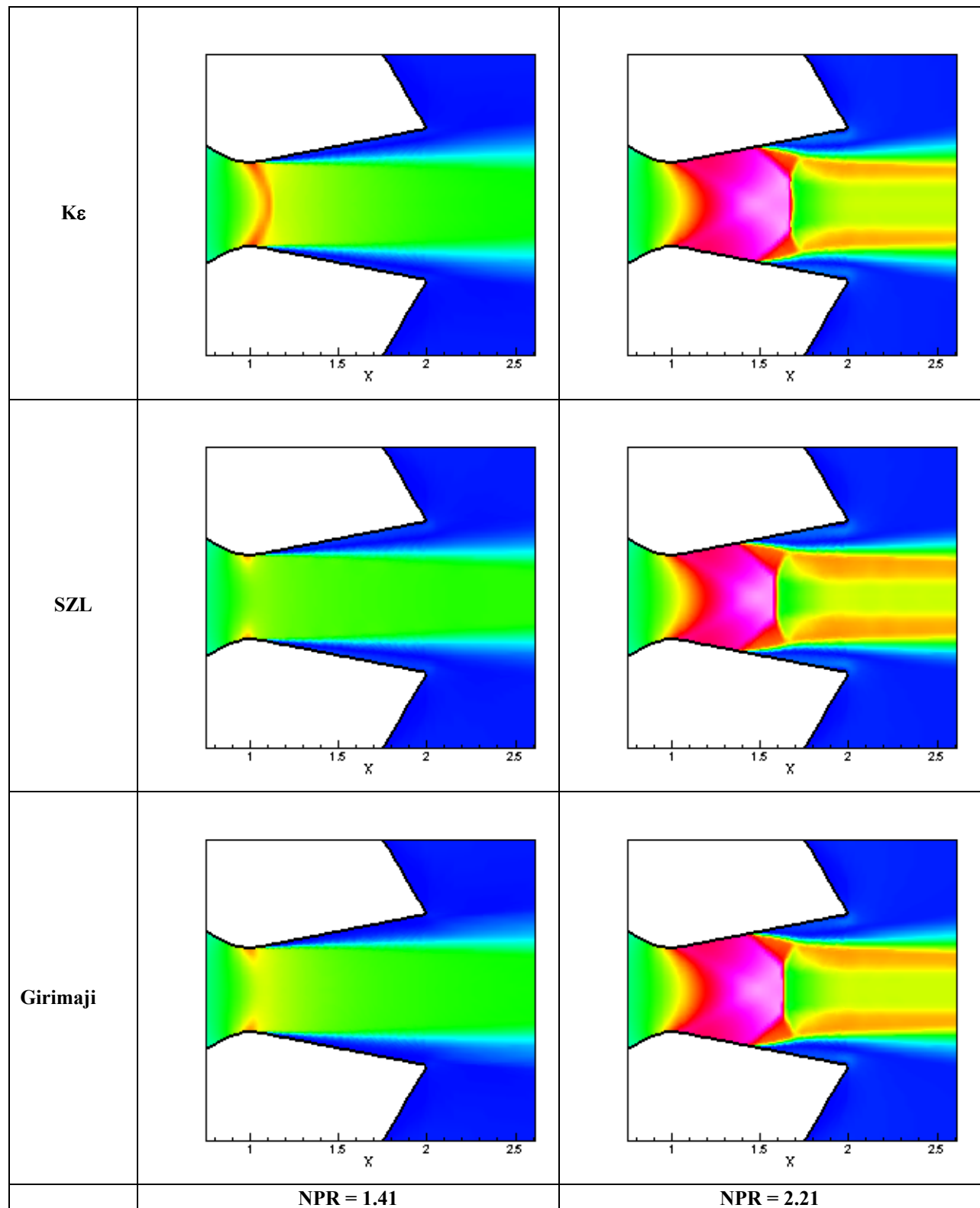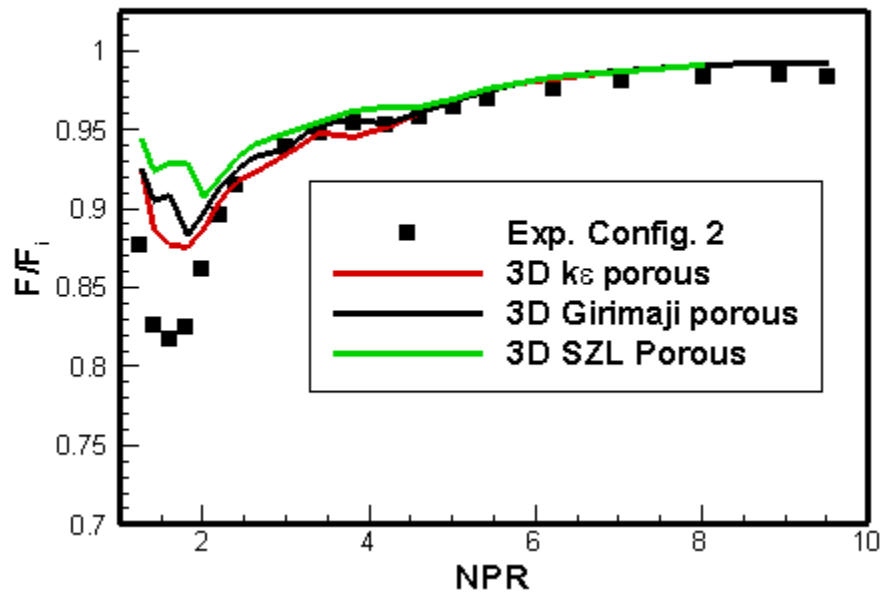| | NPR = 1.41 | NPR = 2.21 |

Figure 10 Mach Contours for baseline configuration at NPR=1.41 And NPR=2.21

Figure 11 Comparison of Nozzle thrust coefficient for baseline configuration using different turbulence models and experimental data of ref (3), 10% Porosity patch
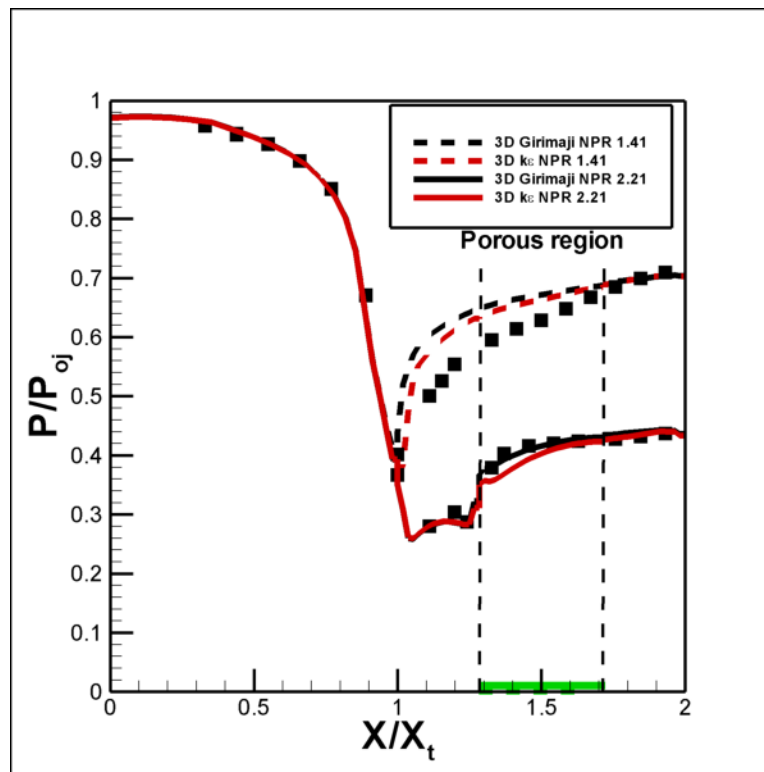

Figure 12 Comparison of turbulence models Computational Pressure Data and Experimental Data of ref (3), 10 % porosity patch
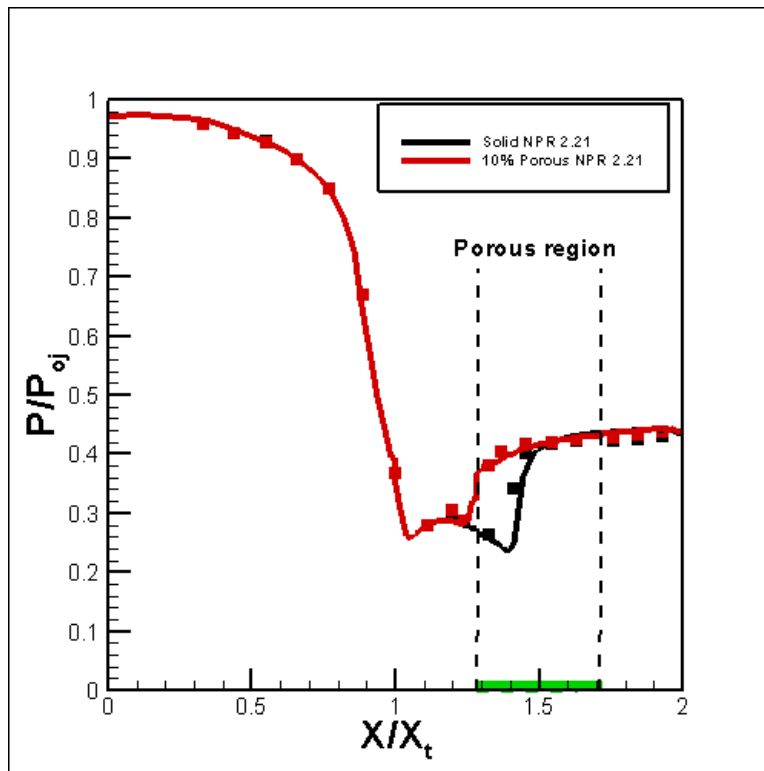
Figure 13 Effect of porosity on internal static pressure ratio distribution at NPR = 2.21